Evaluating the Effects of Graviton Redshift upon Spiral Galaxy Rotation Curves, Surface Brightness Magnitudes and Gravitational Lensing

Firmin J. Oliveira

East Asian Observatory, James Clerk Maxwell Submillimetre Telescope, Hilo, USA
Email: firmjay@hotmail.com

Abstract

The effects of the gravitational redshift of gravitons upon spiral galaxy rotation energy are compared to the standard mass to light analyses in obtaining rotation curves. The derivation of the total baryonic matter compares well with the standard theory and the rotation velocity is matched to a high precision. The stellar mass distributions obtained from the fit with graviton energy loss are used to derive the surface brightness magnitudes for the galaxies, which agree well with the observed measurements. In a new field of investigation, the graviton theory is applied to the observations of gravitational lenses. The results of these applications of the theory suggest that it can augment the standard methods and may eliminate the need for dark matter.

Keywords

Gravitons, Gravitational Redshift, Surface Brightness, Gravitational Lens, Lens Mass

1. Introduction

The theory of the gravitational redshift of gravitons continues to be relevant in the study of galactic phenomena. In this paper the process is investigated at a deeper level in spiral galaxy rotation velocities. It is notable that only the baryonic mass of the galaxy is a free parameter, with other parameters obtained from the observation, essentially just the radial velocity distribution $v(r)$, with the final radial distance r_f and velocity $v(r_f)$ used to determine the graviton coupling coefficient k_f [1].

The SPARC database [2] [3] is used in the spiral galaxy analysis. It provides the baryonic mass, rotational velocity and surface brightness magnitudes for each galaxy. The velocity distributions derived from SPARC mass to light ratio analysis are also presented as a comparison to the Newtonian rotational velocity curves derived using the graviton redshift derived baryonic mass distribution. For the two galaxies presented here, NGC 2403 and NGC 2841, it is notable that the agreement with the standard method is quite good, because the graviton theory derived baryonic mass accounts for the bulge, disk and gas mass without any special adjustments.

In a new field for this theory, gravitational lensing is investigated using Einstein rings [4]. It is found that nothing new needs to be added to the galaxy version of the theory, except that, since galactic rotation velocities were not obtained, the coupling coefficient k_f is determined using the lens mass.

For the layout of this paper, in the next section the rotation velocity relation for spiral galaxies is revisited and the comparisons are made to the predictions of the standard theory. In the section after that, the surface brightness magnitues for those galaxies are considered. In the next section and subsections the gravitational lens relations are described and the connection to the galaxy rotation energy with the graviton redshift energy boost is established. These results are discussed in the final section.

2. Action of Gravitons in Galaxies

The gravitational potential at radial position r in the field of a galaxy of total baryonic mass M_b, including graviton energy loss [1], can be expressed by,

$$\Phi(r) = -\frac{GM(r)}{r} - k_f \frac{M(r)}{M_b} \int_0^r \frac{GM(s)}{s^2} \mathrm{d}s, \tag{1}$$

where $M(r)$ is the baryonic mass within r, and k_f is a coupling coefficient. The negative sign on the second term on the right hand side of Equation (1) represents the energy loss due to the gravitational redshift of gravitons traveling outward against the field of the galaxy of mass $M(r)$ toward an orbiting object of mass m. The equation for the total energy of the mass m in the galaxy is given by,

$$\frac{1}{2}mv^2(r) + m\Phi(r) = E_0, \tag{2}$$

where $v(r)$ is the velocity at r and E_0 is the total energy. For circular motion, $E_0 = -GmM(r)/2r$. The equation for circular motion in the field, from Equation (2), is given by,

$$v^2(r) = \frac{GM(r)}{r} + 2k_f \frac{M(r)}{M_b} \int_0^r \frac{GM(s)}{s^2} \mathrm{d}s. \tag{3}$$

Equation (3) can be put into a form quadratic in the mass $M(r)$, expressed by,

$$v^2(r) = \frac{GM(r)}{r} + 2k_f \frac{M(r)}{M_b} \int_0^{r_1} \frac{GM(s)}{s^2} \mathrm{d}s + 2k_f \frac{(M(r))^2}{M_b} \int_{r_1}^r \frac{G}{s^2} \mathrm{d}s, \tag{4}$$

where, for the last term on the right hand side, the mass $M(r)$ has been taken out of the integral because r_1 is defined such that, for $r_1 < s \le r$, $M(s) \approx M(r)$. Given an estimate for the total galaxy baryonic mass M_b, a mass distribution can be determined [5] by iteratively solving Equation (4) for $M(r)$ until the mean error between the predicted and observed rotational velocities is within acceptable bounds. The galaxy total baryonic mass is obtained from the SPARC mass to light derived velocity estimates for the bulge and disk models and from the independently determined gas mass observations. The baryonic mass is estimated using the final position R and final bulge, disk and gas velocities V_{bulge}, V_{disk} and V_{gas}, respectively, by,

$$M_b = \frac{R}{G}\left(V_{bulge}^2 + V_{disk}^2 + V_{gas}^2\right). \tag{5}$$

Figure 1 shows for galaxy NGC 2403 the rotation velocity curves for the Newtonian, graviton redshift and the combined total velocity fitted to the observed rotation velocities and assumed baryon mass. Also shown on the figure are the rotation curve components for the gas mass and the disk stellar mass based on photometric observations, and the combined Newtonian velocity distribution.
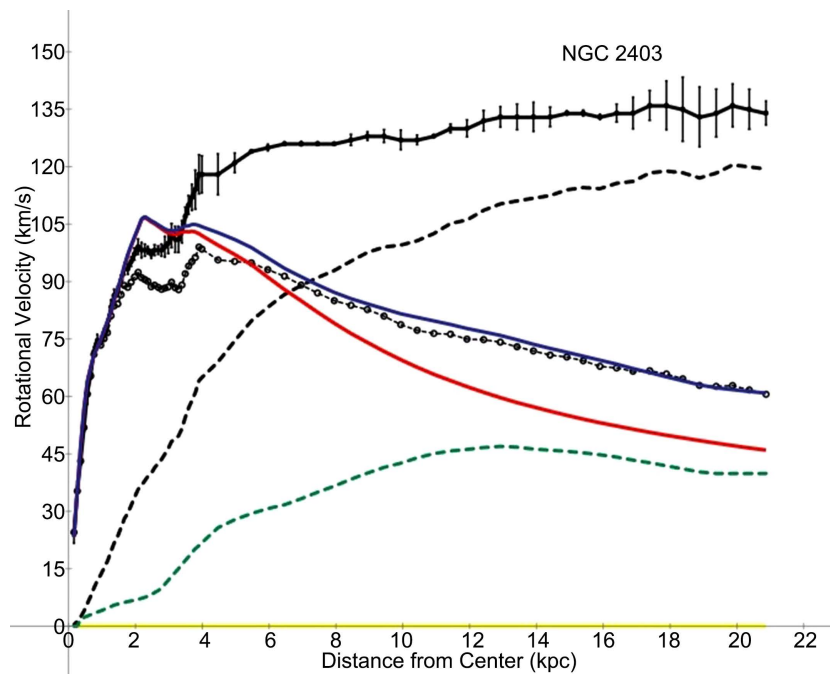

Figure 1. NGC 2403 rotation curves. The black dots with error bars are velocities and errors of the observation data. The solid black line is the Newtonian plus graviton gravitational redshift boosted theoretical circular velocity fit to the observed data. The black dashed line with open circles is the Newtonian velocity curve with the theoretical mass distribution. The dashed black line is the graviton gravitational redshift boosted velocity curve with the theoretical mass distribution. The green dashed line is the observed gas velocity. The yellow line is for the mass estimation of the bulge velocity (zero for this galaxy). The red line is for the mass estimation for the stars in the galaxy. The blue line is the sum of the gas, bulge and star velocities.

Figure 2 shows for galaxy NGC 2841 the rotation velocity curves for the Newtonian, graviton redshift and the combined total velocity fitted to the observed rotation velocities and assumed baryon mass. Also shown on the figure are the rotation curve components for the gas mass and the stellar masses for the bulge and disk based on the photometric observations, and the combined Newtonian velocity distribution. Table 1 summarizes the parameters used in making these galaxy fits.
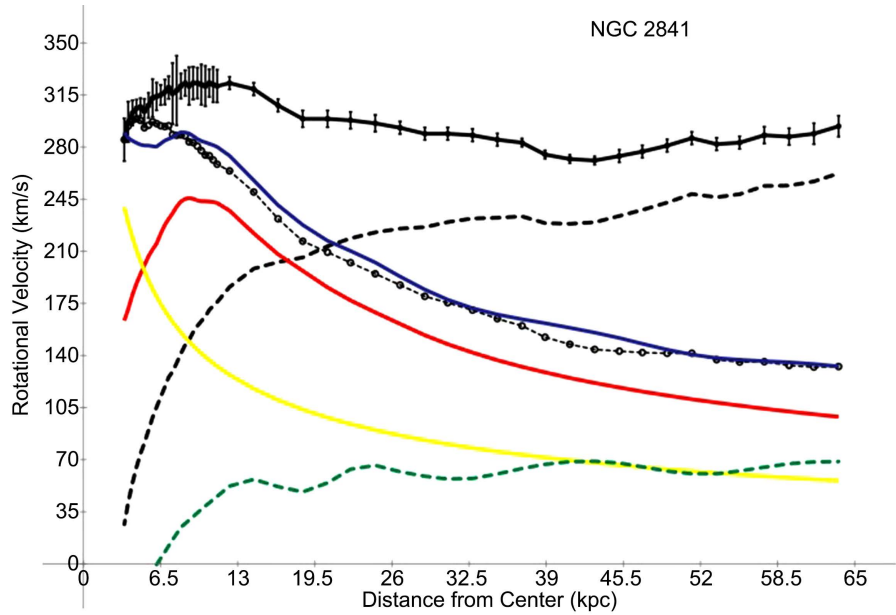

Figure 2. NGC 2841 rotation curves. The black dots with error bars are velocities and errors of the observation data. The solid black line is the Newtonian plus graviton gravitational redshift boosted theoretical circular velocity fit to the observed data. The black dashed line with open circles is the Newtonian velocity curve with the theoretical mass distribution. The dashed black line is the graviton gravitational redshift boosted velocity curve with the theoretical mass distribution. The green dashed line is the observed gas velocity. The yellow line is for the mass estimation of the bulge velocity. The red line is for the mass estimation for the stars in the galaxy. The blue line is the sum of the gas, bulge and star velocities.

Table 1. Spiral galaxy rotational velocity fits.

Galaxy	M_b	V_f	R_f	k_f	Fit Error	B_0	Z_0
	$10^{10}\,M_\odot$	$km \cdot s^{-1}$	kpc		$km \cdot s^{-1}$	10^{23}	mag arcsec^{-2}
NGC 2403	1.797	134	20.87	0.264	0.06	7.5	27.204
NGC 2841	2.604	294	63.64	0.199	0.05	7.5	26.941

3. Surface Brightness

The mass to light ratio $\Upsilon(r)$ within radial position r in a galaxy is based on the observed surface brightness magnitude $\mu(r)$ with source reference μ_0, which is expressed by,

$$\Upsilon(r) = 10^{(\mu(r)-\mu_0)/2.5} \frac{M_{stars}(r)}{4\pi r^2 Area(r,d)B_0}, \tag{6}$$

where B_0 is the detector calibration zero point reference (count), where count ~ energy/time/area, $M_{stars}(r)$ is the mass of the stars within r, given by,

$$M_{stars}(r) = M(r) - \frac{rV_{gas}^2(r)}{G}, \tag{7}$$

where $V_{gas}(r)$ is the molecular gas velocity at r, and the area $Area(r,d)$ in square arcseconds spanned by a radius r of a galaxy at distance d from an observing detector is given by,

$$Area(r,d) = \left(\frac{r}{d}\frac{180}{\pi}3600\right)^2. \tag{8}$$

In terms of Equations (6)-(8), the luminosity $L(r)$ at the radial position r from the center of a galaxy is defined by,

$$L(r) = \frac{M_{stars}(r)}{\Upsilon(r)}. \tag{9}$$

The brightness $B(r)$ is the luminosity thru the surface area defined by,

$$B(r) = \frac{L(r)}{4\pi r^2}. \tag{10}$$

In terms Equations (6)-(10) the surface brightness magnitude $\mu(r)$ is defined by,

$$\mu(r) = -2.5\log\left(\frac{B(r)}{Area(r,d)B_0}\right) + \mu_0, \tag{11}$$

where B_0 is the detector calibration zero point reference count, d is the distance from the observing detector to the source and μ_0 is a source surface brightness reference.

Figure 3 shows for NGC 2403 the surface brightness magnitudes (SB) for the observed and predicted SB fit based on the predicted stellar mass. The reference offset was $Z_0 = 27.204$ to fit to the interpolated curve to the observed SB curve. (The interpolation aligns the observed SB radial positions with the observed galaxy velocity positions.) Figure 4 shows for NGC 2841 the surface brightness magnitudes for the observed and predicted surface brightness magnitudes fit based on the predicted stellar mass. The reference offset was $Z_0 = 26.941$ to fit to the interpolated curve. The detector calibration zero point value used is the same for both results at $B_0 = 7.5 \times 10^{23}$ count per observation.

4. Gravitational Lens Including Interaction of Gravitons with Photons

The gravitational potential $\Phi(r)$ describing the interaction of a photon with a galaxy having total baryonic mass M_b including graviton interacion is defined by,
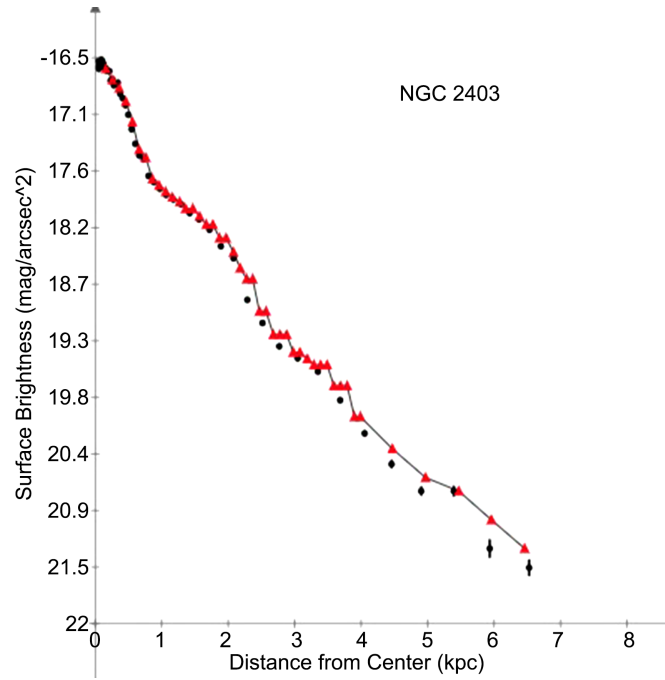
Figure 3. NGC 2403 Surface Brightness Magnitudes. The black dots and error bars are the observed surface brightness magnitudes (SB). The fine black dotted line is the observed SB interpolated to the velocity data radial positions. The red triangles are the SB based on the theoretically derived baryonic mass distribution.

Figure 4. NGC 2841 Surface Brightness Magnitudes. The black dots and error bars are the observed surface brightness magnitudes (SB). The fine black dotted line is the observed SB interpolated to the velocity data radial positions. The red triangles are the SB based on the theoretically derived baryonic mass distribution.
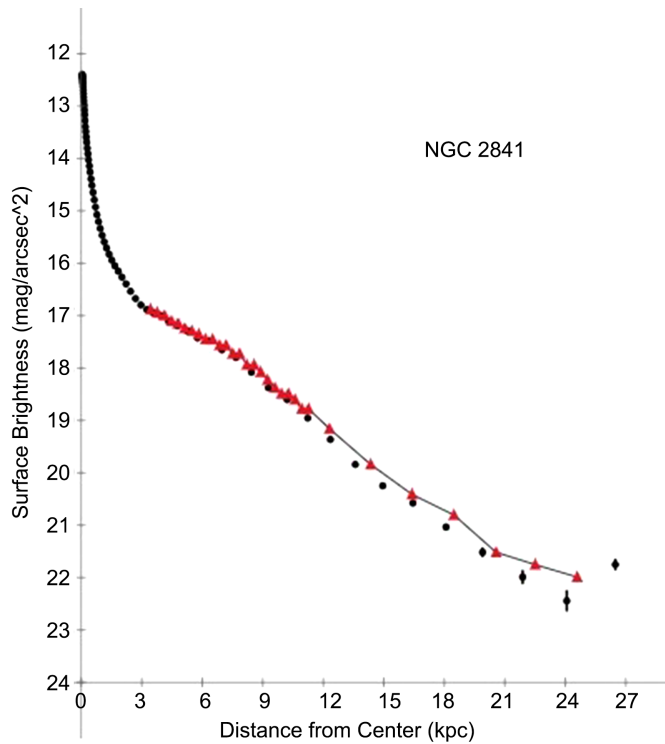
$$\Phi(r) = -\frac{GM_b}{r} + k_g \int_0^r \frac{GM(u)}{u^2} \mathrm{d}u, \tag{12}$$

where G is the gravitational constant, M_b is the total baryonic mass of the galaxy, k_g is the graviton to photon coupling coefficient and $M(r)$ is the baryonic mass at radial position r. The positive value of the second term in Equation (12) indicates it is an increase in the graviton energy (blue shift) as they travel from the photons toward the galaxy mass. The deviation in the path of the photon as it travels from the distant star, passing a distance b at closest approach to the galaxy and continuing on to the detector at the earth is given by [6],

$$\nabla_\perp \Phi(r) = \frac{\partial \Phi(r)}{\partial b} = \frac{\partial \Phi(r)}{\partial r} \frac{\partial r}{\partial b}. \tag{13}$$

Assume,

$$r = \sqrt{b^2 + z^2}, \tag{14}$$

where b is the radial distance from the galaxy center which is beyond the bounds of the galaxy baryonic mass and z is on a line perpendicular to b which extends from the photon source to the observing detector. [1]With this definition of the nearest approach b to the galaxy, assuming $\partial k_g / \partial r = 0$, the derivative of $\Phi(r)$ with respect to r is given by,

$$\frac{\partial \Phi(r)}{\partial r} = \frac{GM_b}{r^2} + k_g \frac{GM(r)}{r^2} = \frac{GM_{lens}}{r^2}, \tag{15}$$

where the lens mass is defined by,

$$M_{lens} = (1 + k_g) M_b, \tag{16}$$

And $M(r) = M_b$ because r is greater than the galaxy radius R_{gal}. The derivative of r with respect to b, using (14), is given by

$$\frac{\partial r}{\partial b} = \frac{b}{r}. \tag{17}$$

Substituting from Equations (15) and (17) into Equation (13) yields,

$$\nabla_\perp \Phi(r) = \frac{bGM_{lens}}{r^3}. \tag{18}$$

Refer to Figure 5 for an illustration of the ray paths associated with a gravitational lens system, where it is shown that the total deflection angle of the photon traveling from the source to the observer is given by,

$$\theta(b) = \alpha(b) + \beta(b). \tag{19}$$

This total deflection angle $\theta(b)$ is obtained initially by integrating Equation (18) along the line z, expressed by,

---

[1]For our purposes it will be assumed that there is no mass in the thin shell region of space around the distance b from the galaxy center, even though graviton redshift generates a relativistic mass in what is traditionally empty space.
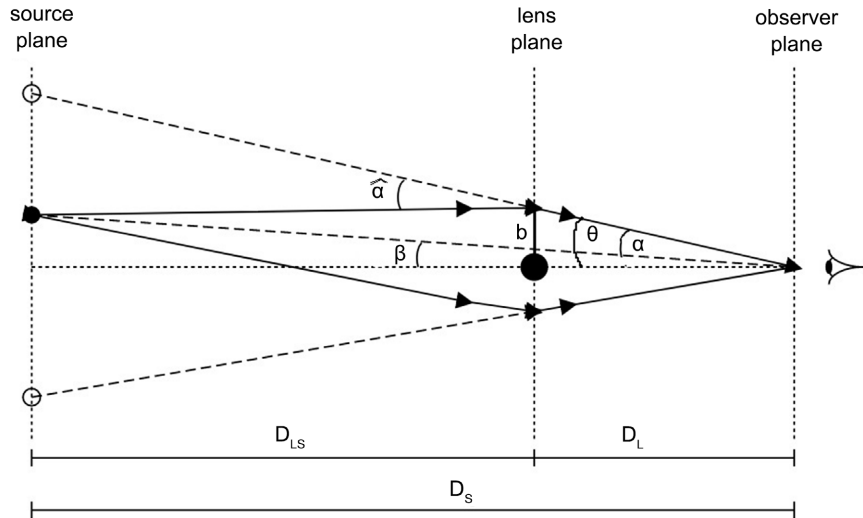
Figure 5. Geometry of the basic gravitational lens system [7].

$$\hat{\alpha}(b) = \frac{2}{c^2} \int_{-\infty}^{\infty} dz \nabla_{\perp} \Phi(r)$$

$$= \frac{2bGM_{lens}}{c^2} \int_{-\infty}^{\infty} \frac{dz}{\left(b^2 + z^2\right)^{3/2}}$$

$$= \frac{2GM_{lens}}{c^2 b} \int_{-\infty}^{\infty} \frac{dx}{\left(1 + x^2\right)^{3/2}} \tag{20}$$

$$= \frac{4GM_{lens}}{c^2 b},$$

where there is a change of variable $x = z/b$. In Equation (20), the first factor of 2 comes from general relativity theory and the second factor of 2 comes from the integral of $dx\left(1 + x^2\right)^{-3/2}$ with x going from $-\infty$ to $+\infty$.

Then, from Equation (20) the angle $\alpha(b)$ is given by,

$$\alpha(b) = \frac{D_{LS}}{D_S} \hat{\alpha}(b) = \frac{D_{LS}}{D_S} \frac{4GM_{lens}}{c^2 b}, \tag{21}$$

where D_L is the angular diameter distance from the observing detector to the lens, D_S is the angular diameter distance from the detector to the source, and D_{LS} is the angular diameter distance from the lens to the source. The impact parameter of the light path to the lens is b, given by

$$b = D_L \theta(b). \tag{22}$$

For a source which is on the center line thru the detector and lens, the angle $\beta(b) = 0$, which, by combining Equations (19), (21) and (22), implies that,

$$\theta(b) = \alpha(b) = \frac{D_{LS}}{D_S} \hat{\alpha}(b) = \frac{D_{LS}}{D_S} \frac{4GM_{lens}}{c^2 D_L \theta(b)}. \tag{23}$$

In this case, where $\beta(b) = 0$, from Equation (23) the angle $\theta_E = \theta(b)$ of the Einstein ring is given by,

$$\theta_E = \sqrt{\frac{D_{LS}}{D_L D_S} \frac{4GM_{lens}}{c^2}}, \tag{24}$$

which is the standard expression. For $\beta(b) \neq 0$, use Equations (19), (21), (22) and (24) to derive the quadratic equation in θ,

$$\theta^2(b) - \beta(b)\theta(b) - \theta_E^2 = 0, \tag{25}$$

which has two solutions,

$$\theta(b)_{\pm} = \frac{1}{2}\left(\beta(b) \pm \sqrt{\beta^2(b) + 4\theta_E^2}\right). \tag{26}$$

4.1. Einstein Ring JWST-ER1r

The gravitational lens system at redshift $z = 1.94$ was detected by the James Webb Space Telescope [8] in 2023 [9]. It is a galaxy of estimated stellar mass $M_b = 1.1 \times 10^{11} M_{\odot}$ (JWST-ER1g). The Einstein ring (JWST-ER1r) subtends an angle of 1.54 arcsec in diameter and is determined to have a radius at the center of the ring of 6.6kpc. The source of the ring is determined to be a galaxy at redshift $z = 2.98$.

The general relativity λ cold dark matter model comoving distance is given by

$$D_c = \frac{c}{H_0} \int_0^z \frac{\mathrm{d}u}{\sqrt{\Omega_M (1+u)^3 + \Omega_\Lambda}}, \tag{27}$$

where H_0 is the Hubble constant, Ω_M is the matter density parameter, Ω_Λ is the mass density parameter due to the cosmological constant and z is the redshift of the source. For this gravitational lens, take $\Omega_M = 0.271$ and $\Omega_\Lambda = 0.729$, with $H_0 = 70\,\mathrm{km \cdot s^{-1} \cdot mpc^{-1}}$. For a situation where there is an intermediate source at redshift z_1 the comoving distance (27) can be expressed,

$$D_c = D_{c1} + D_{c12}, \tag{28}$$

where the comoving distance

$$D_{c1} = \frac{c}{H_0} \int_0^{z_1} \frac{\mathrm{d}u}{\sqrt{\Omega_M (1+u)^3 + \Omega_\Lambda}}, \tag{29}$$

and the comoving distance

$$D_{c12} = \frac{c}{H_0} \int_{z_1}^z \frac{\mathrm{d}u}{\sqrt{\Omega_M (1+u)^3 + \Omega_\Lambda}}. \tag{30}$$

The angular diameter distance DA of the comoving distace D_c at redshift z is defined,

$$DA = \frac{D_c}{1+z}. \tag{31}$$

Similarly the angular diameter distance DA_1 of the comoving distance D_{c1} at redshift z_1 is defined,

$$DA_1 = \frac{D_{c1}}{1+z_1}. \tag{32}$$

Combining Equations (31) and (32) into Equation (28), with some manipulations yields,

$$DA = \frac{(1+z_1)DA_1}{1+z} + \frac{D_{c12}}{1+z},\tag{33}$$

where the angular diameter distance DA_{12} is defined,

$$DA_{12} = \frac{D_{c12}}{1+z}.\tag{34}$$

Substituting Equation (34) into Equation (33) and simplifying to get DA_{12} in terms of the other distances yields,

$$DA_{12} = DA - \frac{1+z_1}{1+z}DA_1.\tag{35}$$

4.2. Derivations for Einstein Ring JWST-ER1r

Regarding JWST-ER1, the angular diameter distance D_L of the lensing galaxy at redshift 1.94, from Equation (27) is given by,

$$D_L = \frac{1}{1+1.94}\frac{c}{H_0}\int_0^{1.94}\frac{du}{\sqrt{0.271(1+u)^3 + 0.729}},\tag{36}$$

where $H_0 = 70.0 \, \text{km}\cdot\text{s}^{-1}\cdot\text{mpc}^{-1}$ and gives a value $D_L = 1.7767\times10^3 \, \text{mpc}$. Likewise, the angular diameter distance D_S of the source at redshift 2.98, from Equation (27) is given by,

$$D_S = \frac{1}{1+2.98}\frac{c}{H_0}\int_0^{2.98}\frac{du}{\sqrt{0.271(1+u)^3 + 0.729}},\tag{37}$$

which gives a value $D_S = 1.6400\times10^3 \, \text{mpc}$. Finally, using Equation (35) the value of the angular diameter distance D_{LS} from the lens to the source at redshift 2.98 is given by,

$$D_{LS} = D_S - \frac{1+1.94}{1+2.98}D_L,\tag{38}$$

which derives a value $D_{LS} = 0.3275\times10^3 \, \text{mpc}$.

The lens mass M_{lens} of galaxy JWST-ER1g is determined by inverting Equation (24),

$$
\begin{aligned}
M_{lens} &= \theta_E^2\frac{D_L D_S c^2}{4GD_{LS}}\\
&= \left(0.77\frac{\pi}{180\times3600}\right)^2\frac{(1.7767\times10^3 \, \text{mpc})(1.6400\times10^3 \, \text{mpc})c^2}{4G(0.3275\times10^3 \, \text{mpc})}\\
&= 6.476\times10^{11} \, \text{M}_\odot.
\end{aligned}\tag{39}
$$

The impact parameter b of the light path at the lens galaxy JWST-ER1g is given by Equation (22), which can be determined using the observed ring diameter angle $\theta = 0.77$ arcsec and the distance D_L to the lens, expressed by

$$
\begin{aligned}
b &= D_L\theta\\
&= 1.7767\times10^3 \, \text{mpc} \times 0.77\frac{\pi}{180\times3600}\\
&= 6.632 \, \text{kpc}.
\end{aligned}\tag{40}
$$

Figure 6 shows the galaxy JWST-ER1g (red circle) and ring (black circle). All angular diameter distances have been double checked for accuracy using the cosmological calculator at [10]. Figure 7 shows the combined mass distributions of the galaxy and ring system, where the dashed blue line is the sum of the stellar mass and dark matter mass, which amounts to just 35% of the lens mass at the distance of the impact parmeter $b = 6.632 \, \text{kpc}$.
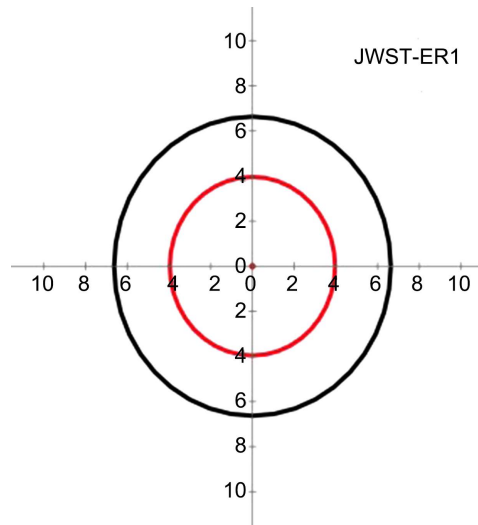

Figure 6. JWST-ER1 galaxy and Einstein ring curves. The solid black circle represents the center of the Einstein ring. The solid red circle represents the bounds of the galaxy.
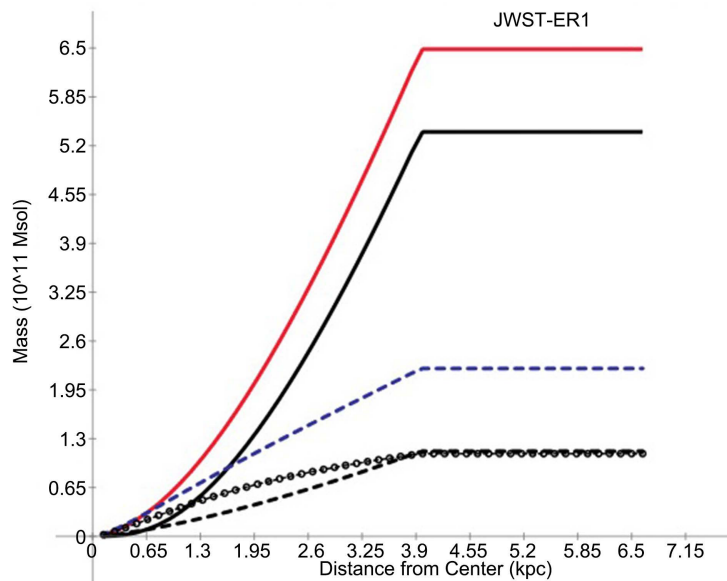

Figure 7. JWST-ER1 mass distribution curves. The black dashed line with open circles is the stellar mass using the Hernquist profile [11], [14]. The solid black line is the graviton redshift mass using the Hernquist profile. The solid red line is the sum of the stellar mass and graviton redshift mass. The dashed black line is the dark matter mass using a simple power law mass distribution as in [12]. The dashed blue line is the sum of the stellar mass and dark matter mass, which amounts to just 35% of the lens mass at the distance of the impact parameter $b = 6.632 \, \text{kpc}$.

4.3. About the Lensing Galaxy JWST-ER1g

For this study assume that the lensing galaxy is an elliptical with a simulated stellar mass distribution based on the Hernquist profile [11], defined in [12] and [13], in the form

$$M(r) = M_*^{Sal} \alpha_{SPS}^{Sal} \left(\frac{r}{R_b}\right)^2 \frac{1 - F(r/R_b)}{(r/R_b)^2 - 1}, \tag{41}$$

where M_*^{Sal} is the stellar (baryonic) mass, α_{SPS}^{Sal} is the Salpeter Stellar Population Synthesis parameter representing the uncertainty of the initial mass function (IMF), R_b is a reference radius based on an effective radius R_e, and $F(u)$ is defined by,

$$F(u) = \frac{1}{\sqrt{1-u^2}} \operatorname{atanh}\left(\sqrt{1-u^2}\right) \text{ if } u < 1,$$
$$= \frac{1}{\sqrt{u^2-1}} \operatorname{atan}\left(\sqrt{u^2-1}\right) \text{ if } u > 1, \tag{42}$$
$$= 1 \text{ if } u = 1.$$

The values for $\alpha_{SPS}^{Sal} = 0.92_{-0.08}^{+0.09}$ are from stellar population studies [12]. The galaxy stellar mass equals M_b within the full galaxy radius $R_{gal} = xR_e$ for some factor x. The dark matter mass profile is provided from [12] for comparative purposes. This is defined as,

$$M_{DM}(r) = M_*^{Sal} A_{DM} \left(\frac{r}{R_e}\right)^{3+\gamma_{DM}}, \tag{43}$$

where A_{DM} and γ_{DM} are parameters determined by best fit from population studies. As described in [12], the best fit parameters for $A_{DM} = M_{DM}(r < R_e)/M_*^{Sal} = 0.21 \pm 0.04$ and for $\gamma_{DM} = -1.60_{-0.13}^{+0.18}$.

The circular velocity $v(r)$ of objects within the galaxy is given by Equation (3), with Newtonian energy and graviton energy redshift,

$$v(r) = \sqrt{\frac{GM(r)}{r} + 2k_f \frac{M(r)}{M_b} \int_0^r \frac{GM(u)}{u^2} du}, \tag{44}$$

where k_f is the graviton coupling coefficient and the baryon mass beyond the galaxy radius R_{gal} is the galaxy total baryon mass,

$$M(r > R_{gal}) = M_b. \tag{45}$$

The total galaxy mass $M_{gal}(r)$ within central distance r, which includes stellar mass, molecular gas mass and graviton redshift mass, from Equation (44), is given by,

$$M_{gal}(r) = M(r) + 2k_f Rx(r) \frac{M(r)}{M_b} \int_0^{Rx(r)} \frac{M(u)}{u^2} du, \tag{46}$$

where $Rx(r) = r$ if $r < R_{gal}$, otherwise $Rx(r) = R_{gal}$. Assuming that the impact parameter b is greater than the full galaxy radius R_{gal}, the lens mass, Equation

(39), equals the galaxy total mass at the galaxy radius R_{gal}, $M_{lens} = M_{gal}\left(R_{gal}\right)$. From Equation (46), setting $r = b$, this is expressed by,

$$M_{lens} = M_{gal}\left(b\right) = M_b + 2k_f R_{gal}\int_0^{R_{gal}}\frac{M\left(u\right)}{u^2}\mathrm{d}u, \tag{47}$$

where the baryon mass $M\left(b\right) = M_b$, the total baryon mass of the galaxy. Equations (39) and (47) imply that,

$$M_{lens} = \theta_E^2\frac{D_L D_S c^2}{4GD_{LS}} = M_{gal}\left(R_{gal}\right) = M_b + 2k_f R_{gal}\int_0^{R_{gal}}\frac{M\left(u\right)}{u^2}\mathrm{d}u, \tag{48}$$

where, in the integral, the stellar mass $M\left(u \geq R_{gal}\right) = M_b$. From Equation (48) an expression for the graviton to photon coupling coefficient k_g defined in Equation (12) is expressed by,

$$k_g = \frac{2k_f R_{gal}}{M_b}\int_0^{R_{gal}}\frac{M\left(u\right)}{u^2}\mathrm{d}u, \tag{49}$$

which ensures that in Equation (15), $\partial k_g/\partial r = 0$ for $r > R_{gal}$. From Eqs. (48) and (49) it is evident that the galaxy mass increase ($k_g M_b$) due to the energy increase of gravitons traveling from the photons into the galaxy resembles the so called dark matter.

This lensing galaxy is at redshift $z_l = 1.94$. The source galaxy which forms the ring is at redshift $z_s = 2.98$. The effective radius of the galaxy is $R_e = 0.46\,\mathrm{arcsec} \times \pi/(180\times3600) \times DL = 3.962\,\mathrm{kpc}$. The Einstein ring radius is $b = \Theta_E \times DL = 0.77\,\mathrm{arcsec} \times \pi/(180\times3600) \times DL = 6.632\,\mathrm{kpc}$. From these parameters, define the galaxy size radial distance $R_{gal} = 1\times R_e = 3.962\,\mathrm{kpc}$. The radius parameter $R_b = 0.511\times R_e = 2.025\,\mathrm{kpc}$. The stellar mass of the galaxy is estimated to be $M_*^{Sal} = 1.10\times10^{11}\,\mathrm{M_\odot}$.

Figure 8 shows the graviton redshift theoretical components of the rotation velocities for galaxy JWST-ER1 [9]. The velocity distributions of the Newtonian rotation curve (black dashed line with open circles), the graviton redshift boost to the velocity curve (black dashed line) and the sum of these curves (solid black line) forming the predicted rotational velocity curve for massive objects rotating in the galaxy.

Two other lens systems with Einstein rings are analysed, by the same methods as for JWST-ER1, from the COSMOS field [15]. These are COSMOS 5921 + 0638 [16] at a redshift $z_l = 0.551$, and COSMOS 0018 + 3845 [15] at a redshift $z_l = 0.9755$. For both of these systems the cosmological parameters used were $H_0 = 70\,\mathrm{km\cdot s^{-1}\cdot mpc^{-1}}$, $\Omega_M = 0.3$ and $\Omega_\Lambda = 0.7$.

Figures 9-11 show the results for COSMOS 5921 + 0638. The solid red line on Figure 10 is the sum of stellar and graviton redshift masses, and the dashed blue line is for the stellar plus dark matter masses, which amounts to 100% of the lens mass for both methods at the distance of the impact parameter $b = 4.621\,\mathrm{kpc}$. It is remarkable that the graviton redshift fit is quite similar to the standard dark matter fit.
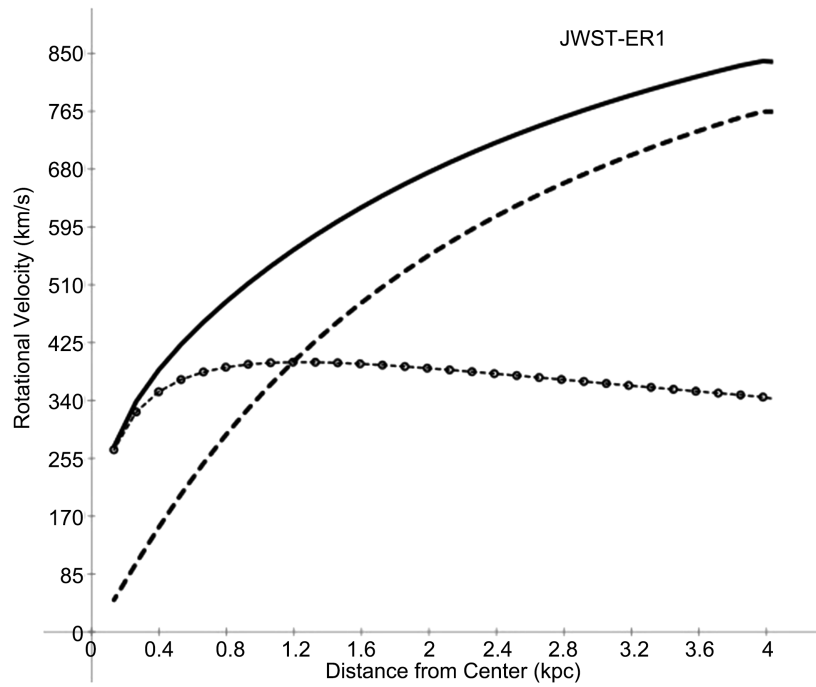
Figure 8. JWST-ER1 rotational velocity distribution curves using the Hernquist profile [12]. The black dashed line with open circles is the Newtonian velocity curve. The black dashed line is the graviton gravitational redshift boosted velocity curve. The solid black line is the Newtonian plus graviton gravitational redshift boosted theoretical circular velocity.
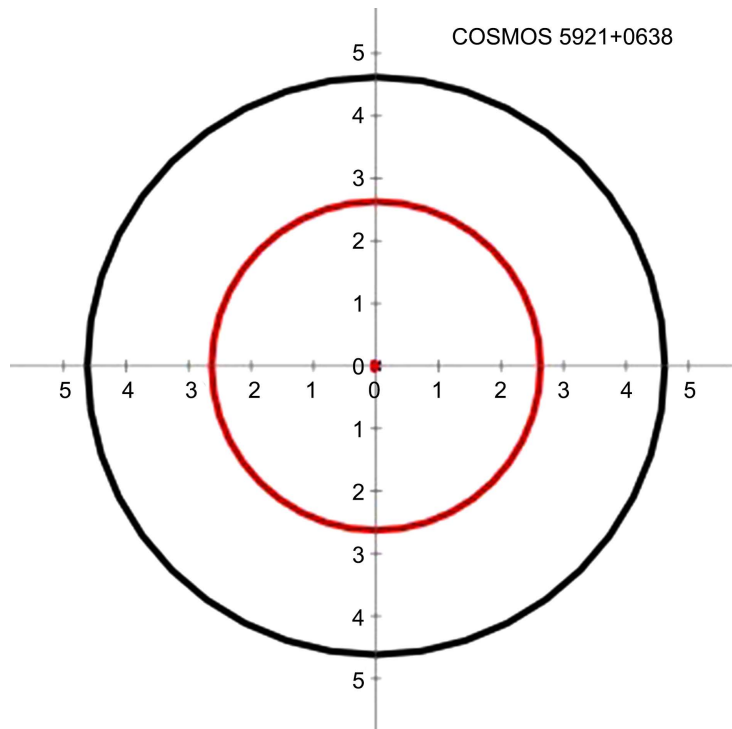

Figure 9. COSMOS 5921 + 0638 galaxy and Einstein ring curves. The solid black circle represents the center of the Einstein ring. The solid red circle represents the bounds of the galaxy.
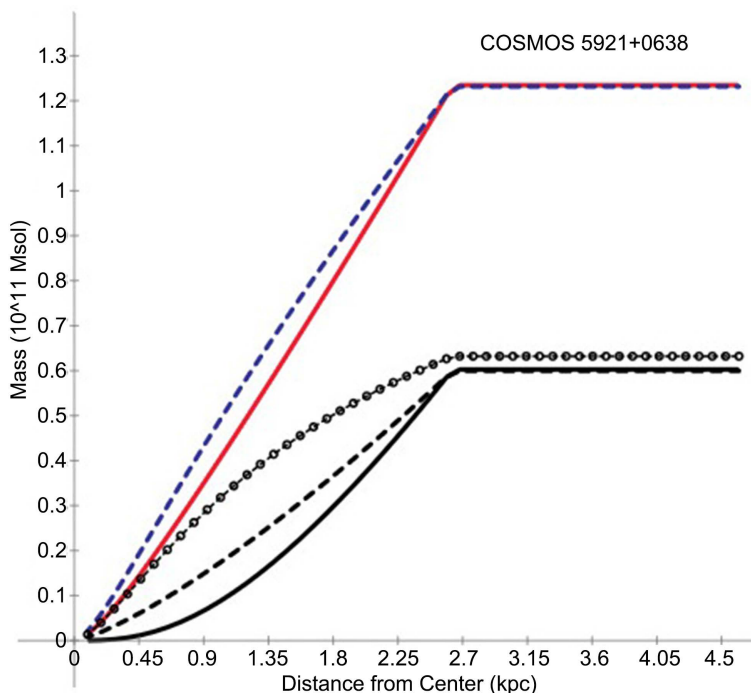
Figure 10. COSMOS 5921 + 0638 mass distribution curves. The black dashed line with open circles is the stellar mass using the Hernquist profile [11] [14]. The solid black line is the graviton redshift mass using the Hernquist profile. The solid red line is the sum of the stellar mass and graviton redshift mass. The dashed black line is the dark matter mass using a simple power law mass distribution as in [12]. The dashed blue line is the sum of the stellar mass and dark matter mass, which amounts to 100% of the lens mass at the distance of the impact parameter $b = 4.621\,\text{kpc}$.
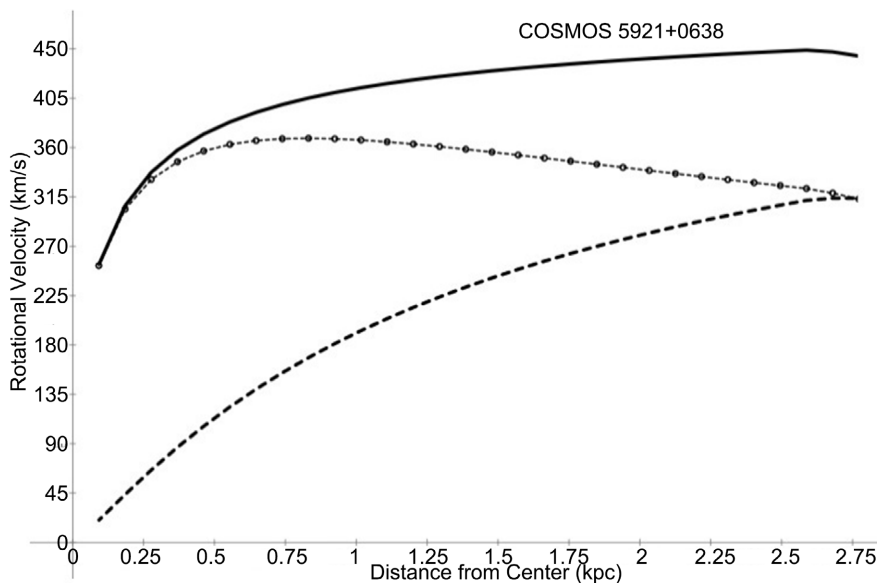

Figure 11. COSMOS 5921 + 0638 rotational velocity distribution curves using the Hernquist profile [12]. The black dashed line with open circles is the Newtonian velocity curve. The black dashed line is the graviton gravitational redshift boosted velocity curve. The solid black line is the Newtonian plus graviton gravitational redshift boosted theoretical circular velocity.

The results for COSMOS 0018 + 3845 are shown in **Figures 12-14**. The dashed blue line on **Figure 13** is the sum of the stellar mass and dark matter mass, which amounts to just 18% of the lens mass at the distance of the impact parmeter $b = 10.508 \text{ kpc}$.

Tables 2-5 show the parameters used and results obtained for the analysis of all three lenses.
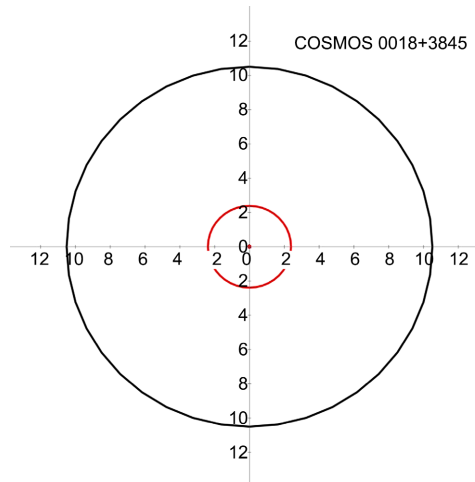

Figure 12. COSMOS 0018 + 3845 galaxy and Einstein ring curves. The solid black circle represents the center of the Einstein ring. The solid red circle represents the bounds of the galaxy.
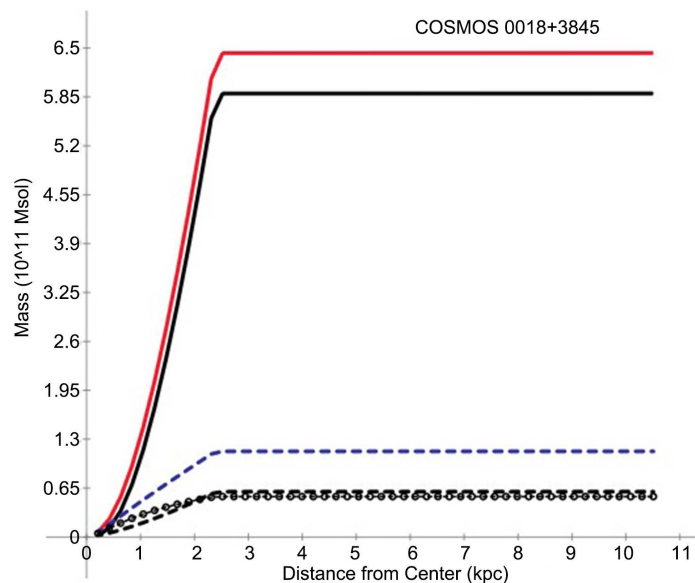

Figure 13. COSMOS 0018 + 3845 mass distribution curves. The black dashed line with open circles is the stellar mass using the Hernquist profile [11], [14]. The solid black line is the graviton redshift mass using the Hernquist profile. The solid red line is the sum of the stellar mass and graviton redshift mass. The dashed black line is the dark matter mass using a simple power law mass distribution as in [12]. The dashed blue line is the sum of the stellar mass and dark matter mass, which amounts to just 18% of the lens mass at the distance of the impact parameter $b = 10.508 \text{ kpc}$.
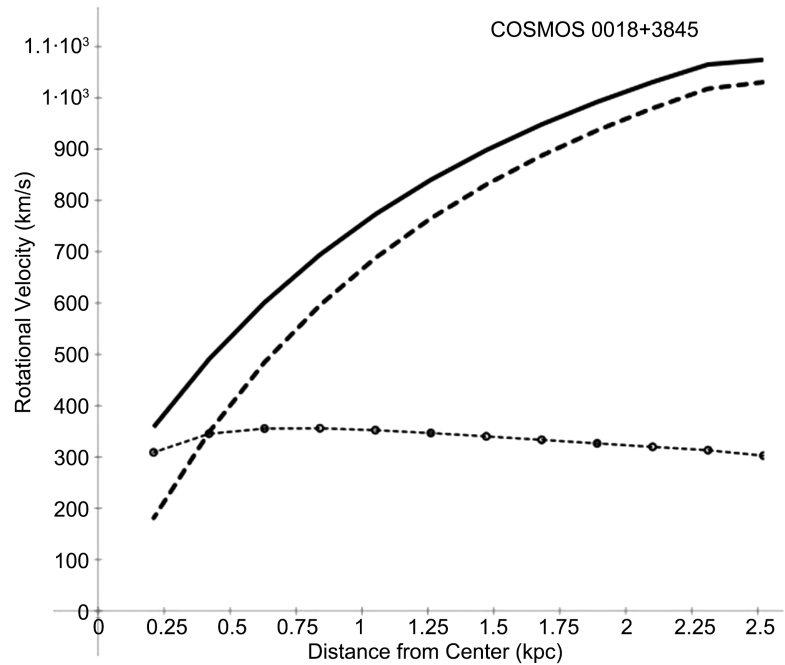
Figure 14. COSMOS 0018 + 3845 rotational velocity distribution curves using the Hernquist profile [12]. The black dashed line with open circles is the Newtonian velocity curve. The black dashed line is the graviton gravitational redshift boosted velocity curve. The solid black line is the Newtonian plus graviton gravitational redshift boosted theoretical circular velocity.

Table 2. Lens galaxy parameters.

Galaxy	H_0	Ω_M	Ω_Λ	Z	Z
	km·s⁻¹·mpc⁻¹			Lens	Source
JWST-ER1	70	0.271	0.729	1.94	2.98
COSMOS 5921 + 0638	70	0.3	0.7	0.551	3.14 2
COSMOS 0018 + 3845	70	0.3	0.7	0.9755	3.96

Table 3. Lens galaxy parameters.

Galaxy	DL	DS	DLS
	10^3 mpc	10^3 mpc	10^3 mpc
JWST-ER1	1.777	1.640	0.3275
COSMOS 5921 + 0638	1.324	1.567	1.071
COSMOS 0018 + 3845	1.642	1.440	0.7860

Table 4. Lens galaxy parameters.

Galaxy	M_b	M_{lens}	R_e	b	α_{SPS}^{Sal}	A_{DM}	γ_{DM}
	10^{10} M$_\odot$	10^{11} M$_\odot$	kpc	kpc			
JWST-ER1	11.0	6.476	3.962	6.632	1.002	0.21	−1.60
COSMOS 5921 + 0638	6.32	1.233	2.631	4.621	0.92	0.19	−1.70
COSMOS 0018 + 3845	5.37	6.436	2.388	10.508	0.92	0.21	−1.60

Table 5. Lens galaxy parameters.

Galaxy	Θ_E	M_*^{Sal}	R_b	R_{gal}	k_f	k_g
	arcsec	$10^{11}\,M_\odot$	kpc	kpc		
JWST-ER1	0.77	1.10	2.025	3.962	0.541	4.887
COSMOS 5921 + 0638	0.72	1.32	1.345	2.631	0.1055	0.950
COSMOS 0018 + 3845	1.32	1.12	1.220	2.388	1.215	10.984

5. Discussion

The fitting of spiral galaxy rotation curves using the theory of graviton gravitational redshift in the galaxy field may be perceived as not adding anything new to the explanation of high velocity rotations which flatten out at large radial distances, since these are adequately explained by other dark matter theories, particularly, in principle, in the framework of extended gravity [17], although gravitons are more likely to exist than dark matter particles and the graviton redshift theory can explain binary star system decay without the emission of gravitational waves [18]. Also, showing how the stellar mass distribution derived from the graviton redshift method can be used to explain the galaxy surface brightness magnitudes does not offer anything extraordinary.

However, it is in gravitational lensing where this theory may have revealed its significance, because it has been shown how the graviton redshift theory can explain the lens mass when dark matter theory cannot, as in the cases of the ring systems in JWST-ER1 and COSMOS 0018 + 3845. The fundamental property about graviton gravitational redshift is that the total galaxy mass $M_{gal}(r) \propto r$ at large distance, since the gravitational redshift continues to act at larger distance r and add more relativistic mass to the system. Assume that most of the baryonic mass M_b is within a radius $R_e \leq R_{gal}$. Then, for $r > R_e$, expand Equation (48) into the form,

$$M_{gal}(r > R_e) \approx M_b + 2k_f r \left(\int_0^{R_e} \frac{M(u)}{u^2}\,du + M_b \int_{R_e}^{r} \frac{du}{u^2} \right)$$
$$= M_b + 2k_f r \left(\frac{M_b}{R_a} + \frac{M_b}{R_e} - \frac{M_b}{r} \right) \qquad (50)$$
$$= (1 - 2k_f)M_b + Br,$$

where $\dfrac{M_b}{R_a} - \displaystyle\int_0^{R_e} \dfrac{M(u)}{u^2}\,du$ for some distance R_a and $B = 2k_f M_b \left(\dfrac{1}{R_a} + \dfrac{1}{R_e} \right)$.

All of the lens systems in this study displayed this approximately $M_{gal}(r) \propto r$ relation, although the integrations were terminated at the galaxy radius R_{gal}. The behavior of extending the graviton interaction distance beyond the galaxy radius would result in a stream of concentric rings at the lens site from a single source beyond the lens galaxy (or galaxy cluster.) This needs further study.

Conflicts of Interest

The author declares no conflict of interest.

References

[1] Oliveira, F.J. (2022) How the Redshift of Gravitons Explains Dark Matter and Dark Energy. *Journal of Modern Physics*, **13**, 1348-1368. https://doi.org/10.4236/jmp.2022.1311084

[2] http://astroweb.cwru.edu/SPARC/

[3] Lelli, F., McGaugh, S.S. and Schombert, J.M. (2016) SPARC: Mass Models for 175 Disk Galaxies with Spitzer Photometry and Accurate Rotation Curves. *The Astronomical Journal*, **152**, 157-170. https://doi.org/10.3847/0004-6256/152/6/157

[4] Einstein, A. (1952) The Foundation of the General Theory of Relativity. Dover.

[5] Oliveira, F.J. (2023) New Insights into the Action of Gravitons in Spiral Galaxies. *Journal of High Energy Physics, Gravitation and Cosmology*, **9**, 968-983. https://doi.org/10.4236/jhepgc.2023.94072

[6] Pritchard, J. (2009) Lecture Notes: Gravitational Lensing. https://lweb.cfa.harvard.edu/~dfabricant/huchra/ay202/lectures/lecture12.pdf

[7] File: Gravitational Lens Geometry.svg. https://commons.wikimedia.org/w/index.php?curid=20298731

[8] https://webbtelescope.org/home

[9] van Dokkum, P., Brammer, G., Wang, B., Leja, J. and Conroy, C. (2023) A Massive Compact Quiescent Galaxy at Z = 2 with a Complete Einstein Ring in JWST Imaging. *Nature Astronomy*, **8**, 119-125. https://doi.org/10.1038/s41550-023-02103-9

[10] Wright, E.L. (2006) A Cosmology Calculator for the World Wide Web. *Publications of the Astronomical Society of the Pacific*, **118**, 1711-1715. https://doi.org/10.1086/510102

[11] Hernquist, L. (1990) An Analytical Model for Spherical Galaxies and Bulges. *The Astrophysical Journal*, **356**, 359-364. https://doi.org/10.1086/168845

[12] Oguri, M., Rusu, C.E. and Falco, E.E. (2014) The Stellar and Dark Matter Distributions in Elliptical Galaxies from the Ensemble of Strong Gravitational Lenses. *Monthly Notices of the Royal Astronomical Society*, **439**, 2494-2504. https://doi.org/10.1093/mnras/stu106

[13] Bruzual, G. and Charlot, S. (2003) Stellar Population Synthesis at the Resolution of 2003. *Monthly Notices of the Royal Astronomical Society*, **344**, 1000-1028. https://doi.org/10.1046/j.1365-8711.2003.06897.x

[14] Keeton, C.R. (2001) A Catalog of Mass Models for Gravitational Lensing. arXiv: astro-ph/0102341.

[15] Faure, C., Anguita, T., Alloin, D., Bundy, K., Finoguenov, A., Leauthaud, A., *et al.* (2011) On the Evolution of Environmental and Mass Properties of Strong Lens Galaxies in Cosmos. *Astronomy & Astrophysics*, **529**, A72. https://doi.org/10.1051/0004-6361/200913498

[16] Anguita, T., Faure, C., Kneib, J.-., Wambsganss, J., Knobel, C., Koekemoer, A.M., *et al.* (2009) COSMOS 5921 + 0638: Characterization and Analysis of a New Strong Gravitationally Lensed AGN. *Astronomy & Astrophysics*, **507**, 35-46. https://doi.org/10.1051/0004-6361/200912091

[17] Corda, C. (2009) Interferometric Detection of Gravitational Waves: The Definitive Test for General Relativity. *International Journal of Modern Physics D*, **18**, 2275-2282. https://doi.org/10.1142/s0218271809015904

[18] Oliveira, F.J. (2022) Binary Star System Decay by Graviton Interaction. *Journal of High Energy Physics, Gravitation and Cosmology*, **8**, 317-329. https://doi.org/10.4236/jhepgc.2022.82026